Modelling and Characterization of an Electro-Thermal MEMS Device for Gas Property Determination

Philipp Raimann
Hahn-Schickard
Villingen-Schwenningen, Germany
philipp.raimann@hahn-schickard.de

Frank Hedrich
Hahn-Schickard
Villingen-Schwenningen, Germany
frank.hedrich@hahn-schickard.de

Sophie Billat
Hahn-Schickard
Villingen-Schwenningen, Germany
sophie.billat@hahn-schickard.de

Alfons Dehé
Georg H. Endress Chair for Smart Systems Integration,
University of Freiburg
Villingen-Schwenningen, Germany
dehe@imtek.uni-freiburg.de

***Abstract* — The increasing requirements for monitoring of gas composition e.g. in fuel gas control have led to a strong demand for cost-effective gas sensing solutions. This work presents the modelling and characterization of a miniaturized thermal gas sensor. In the proposed measurement technique, a polysilicon heater placed on a thin membrane is excited with a periodic heating voltage and the resulting temperature response is evaluated in the frequency domain using thermopiles and a lock-in amplifier. The thermo-physical properties of the surrounding gas alters the heat loss of the heating element to the environment leading to a gas-specific thermal characteristic. A thermal lumped element model interprets amplitude and phase of the thermopile signal yielding the estimation of thermal conductivity and volumetric heat capacity. The simultaneous and selective measurement of these two independent thermal properties offers the possibility to improve the performance of existing thermal gas sensors. We were able to distinguish gases over a wide range of properties with high reproducibility based on our thermal model.**

Keywords— MEMS, Gas Sensor, Thermal Modelling, Lock-in amplifier

I. INTRODUCTION

Measurements of gas concentrations are becoming increasingly important in medical, industrial and environmental applications requiring reliable sensors with high sensitivity, selectivity and specificity. [1-4]. In recent decades, significant improvements in manufacturing technologies have led to microsystems with high gas sensing performances. Currently, metal-oxide sensors [5-7] and novel organic-based chemo-resistive sensors [8, 9], which rely on chemical interactions between the gas and a chemically active target material, dominate the market and nowadays research activities because of their potential in resolving the lowest gas concentrations (<10 ppm) [10, 11]. However, high power consumption due to high operating temperatures of metal-oxide sensors, slow response times, various cross-sensitivities as well as a limited measuring range and long-term stability restrict the areas of application [5, 9]. Optical sensors based on the absorption of light do have a wide measuring range and offer resolutions well below 100 ppm, but are difficult to miniaturized, quite expensive and suffer from a high power consumption [12-15].

However, some applications (e.g., hydrogen safety warning in automotive applications and fuel gas metering) require miniaturized low-power sensor systems with fast response times, low manufacturing costs, high reliability and long-term stability and do have minor demands to sensitivity. Here, electro-thermal gas sensors, which measure the thermal interaction between a heated element and its surrounding gas medium, are very attractive. Unfortunately, thermal gas detection methods are intrinsically non-selective, since only the physical properties of the surrounding can be detected and require additional cross-sensitivity compensation for ambient parameters [16, 17]. Currently, miniaturized thermal conductivity sensors are employed for the detection of hydrogen in safety applications, since the thermal conductivity differs significantly from air [18, 19]. However, it is possible to distinguish gases based on other thermal parameters (Tab. 1). In order to determine these fluid properties, transient methods with pulses [20], or periodic excitation signals [16, 21, 22] are used. In [16], a sensor with freestanding micro wires is presented, which is able to measure the thermal diffusivity of the surrounding gas in order to better distinguish N_2 and CO_2. Nevertheless, to optimize the sensing performance, it is advisable to determine more than an individual gas property with a single structure. For this purpose, studies of the thermal device characteristic in the frequency domain have been carried out recently. By matching the frequency-dependent thermal response of a simple, single suspended wire with an analytical model, the thermal conductivity and thermal diffusivity of the surrounding gas can be determined [23, 24]. In [22], an analytical model for the measurement of thermal conductivity and diffusivity of liquids is reported, where spatially spaced resistive sensors on a membrane monitor the temperature of the heater. Here, Kuntner et al. assume that the influence of the membrane is negligible, since the dynamic thermal behavior of the fluid dominates. This simplification may be appropriate for liquids, but since most gases have significantly lower thermal conductivities and higher thermal diffusivities than liquids, the effect of the sensor's material properties cannot be ignored.

TABLE I. THERMO-PHYSICAL GAS PROPERTIES AT T= 293 K AND P= 1 BAR. [25]

Gas	Thermal Conductivity *k* ($mW\ m^{-1}\ K^{-1}$)	Volumetric Heat Capacity *cv* ($kJ\ m^{-3}\ K^{-1}$)	Thermal Diffusivity *a* ($cm^2\ s^{-1}$)
CO_2	16.2	1.536	0.106
Ar	17.5	0.855	0.205
N_2	25.5	1.197	0.213
He	153.5	0.852	1.801
H_2	183.4	1.181	1.553

This paper evaluates the impact of varying gas parameters on the thermal response of a membrane-based micro machined sensor and analyzes thermal characteristic of the sensing structure with a lumped element model. In the past, lumped models of thermal systems were used to theoretically describe the sensing performance [17, 26] and to statically determine the thermal resistance of different materials [27]. However, the effects of the gas surrounding the heating elements were often disregarded [28] or insufficiently considered [29]. In this work, we study the influence of varying gas properties on the equivalent parameters of a thermal lumped model. For this purpose, a MEMS-device consisting of a polysilicon heater on a silicon nitride membrane is used. The heater is excited with a periodic voltage signal and the resulting gas-specific temperature amplitudes and phase shifts are monitored with thermopiles consisting of polysilicon and aluminum. For the estimation of thermal conductivity and volumetric heat capacity, this paper applies a model fit on the thermal response of the microstructure. These thermo-physical gas properties have the advantage of varying sensitivity to temperature and pressure offering an opportunity to minimize undesired cross-sensitivities for ambient parameters as well as an improvement of measurement accuracy and gas specificity. In addition, by measuring the independent gas properties, improved sensitivity and selectivity can be achieved, and thus gas-sensing performance may be fundamentally enhanced.

II. FABRICATION

MEMS technologies are ideally suited for the fabrication of thermal sensor in order to achieve high sensitivities and low response times, since selective etching processes create thin, thermally insulated areas that form the active structure of the device [22, 30]. The presented sensor is based on the manufacturing technology of our thermal flow sensor [31] with minor improvements and was realized in the in-house clean room. The process flow is shown in figure 1 and starts with the deposition of an oxide layer, followed by an LPCVD silicon nitride layer. Polysilicon and aluminum are then deposited and structured. Afterwards, these structures are passivated with a PECVD silicon nitride layer. In the next step, the heater is perforated and then the membrane is exposed from the backside with a dry etch process to obtain a high thermal insulation. The perforation of the heater allows gas exchange between the front side and the cavity. This prevents the formation of pressure differences, which positively affects the device's mechanical stability. The hot junctions of the Al-polysilicon thermopiles are placed near the heater, while the cold junctions are located outside the cavity (Fig. 2). Compared to the commonly applied measurements of temperature-dependent electrical resistances [16, 20-24], the temperature detection with thermopiles allows higher

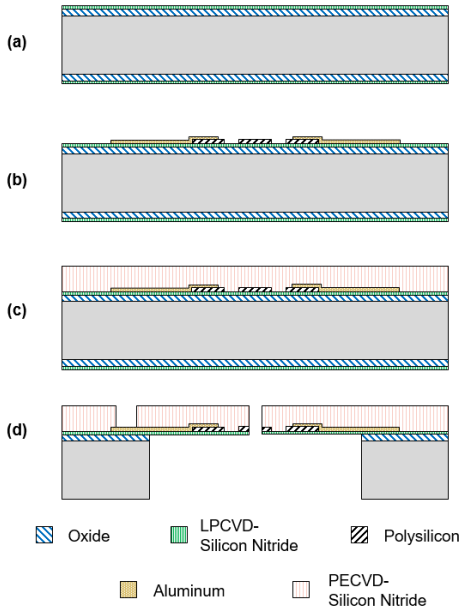

Fig. 1. Overview of the fabrication process steps: (a) Deposition of oxide an LPCVD Si_3N_4, (b) Deposition and patterning of polysilicon and aluminum, (c) Deposition of PECVD Silicon Nitride and (d) Patterning and backside DRIE.

sensitivity and a self-generated signal proportional to the respective excess temperature without the need of biasing. The arrangement of the thermopiles also makes the device less sensitive to changes in ambient conditions, since only the temperature difference between the heated element and the cold bulk silicon is monitored.

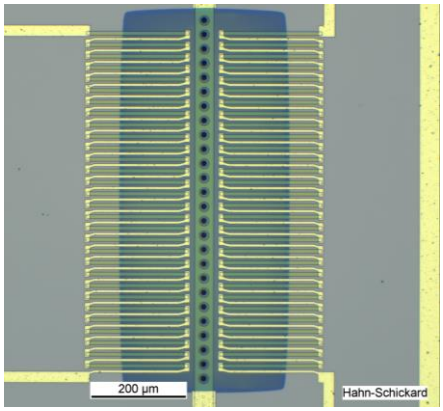

Fig. 2. Fabricated thermal gas sensor featuring the perforated heater and the thermopiles for direct monitoring of the gas-specific heat loss.

III. THERMAL MODEL

For the measurement of the thermo-physical gas properties, a periodic voltage U with an amplitude $\hat{u}_{heater}$ and a frequency *f* is applied.

$$U(t) = \hat{u}_{heater} \cdot \cos(2 \cdot \pi \cdot f \cdot t) \quad (1)$$

The applied voltage generates a power dissipation *P* due to the electrical resistance R_0 within the suspended heating element. This power signal has the form

$$P = \frac{U(t)^2}{R_0} = \frac{\hat{u}_{heater}^{\ 2}}{2 \cdot R_0} + \frac{\hat{u}_{heater}^{\ 2}}{2 \cdot R_0} \cdot \cos(4 \cdot \pi \cdot f \cdot t) \quad (2)$$

and can be separated into a constant time-independent component and an oscillating part. Because of the electrical power dissipation the polysilicon strip heats up. The resulting temperature response is influenced by the heat loss through the gas and the solid materials of the MEMS device. Since the derivation of an exact analytical solution of the heat transfer phenomena in a complex three-dimensional device is extremely time consuming and difficult, we use a lumped system analysis to describe the influence of the thermal gas properties (Fig. 3). In this modeling technique, it is necessary to decompose the device into suitable sub-structures and to define lumped elements. This is done with equivalent resistances and capacitances, which describe the dominant process of heat conduction [21, 22, 29].

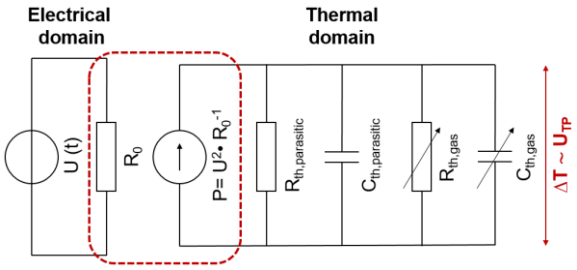

Fig. 3. Simplified thermal lumped model consisting of the parasitic and gas-independent equivalent parameters ($R_{th,parasitic}$ and $C_{th,parasitic}$) as well as the gas-dependent equivalent parameters ($R_{th,gas}$ and $C_{th,gas}$). This approach allows the analysis of different gas properties on the excess temperature ΔT of the heater with an electrical resistance R_0.

Our modeling approach ignores spatial temperature variations within the heater and assumes that the resulting temperature increase can be directly monitored with the thermopiles due to their small distance to the heating element. We also disregard the temperature coefficient of resistance of the polysilicon heater so that the applied power is constant. According to our equivalent circuit (Fig. 3), a low-pass behavior of the sensor is to be expected with the lumped parameters thermal resistance R_{th} and thermal capacitance C_{th} depending on the respective characteristic lengths L, cross-sectional areas A and volumes V as well as on the thermal conductivity k and volumetric heat capacity cv.

$$R_{th,i} = \frac{L_i}{k_i \cdot A_i} \tag{3}$$

$$C_{th,i} = cv_i \cdot V_i \tag{4}$$

The steady-state temperature ΔT_{DC} is exclusively influenced by the parasitic thermal resistance $R_{th,parasitic}$ (e.g. passivation layer, thermopiles, heater) and the thermal gas resistance $R_{th,gas}$. This excess temperature is superimposed by an temperature amplitude ΔT_{AC} at twice the excitation frequency which is additionally effected by the respective thermal masses $C_{th,parasitic}$ and $C_{th,gas}$. In this case, the temperature amplitude is described by equation 5.

$$\Delta T_{AC} = \frac{P}{\sqrt{\left(\frac{1}{R_{th}}\right)^2 + (2 \cdot \pi \cdot f \cdot C_{th})^2}} \tag{5}$$

The temperature signal ΔT_{AC} also exhibits a time delay with respect to the electrical excitation signal. This phase shift Θ is given by:

$$\theta = -\arctan(2 \cdot \pi \cdot f \cdot R_{th} \cdot C_{th}) \tag{6}$$

Basically the thermopile amplitudes $U_{Tp,DC}$ and $U_{Tp,AC}$ or the phase shift Θ of the $U_{Tp,AC}$ signal can be used in order to deduce the two gas properties. In this work, we solely evaluate the amplitude and phase of the $U_{Tp,AC}$ signal. For a precise determination of the gas properties by evaluating the excess temperatures of the heater, it is necessary to know the applied power and the sensitivity of the thermopiles precisely. However, the evaluation of the amplitude has the advantage that it can be divided into a frequency-dependent and frequency-independent part (Eq. 5). This separation enables an individual determination of the thermal conductivity and volumetric heat capacity when performing a frequency scan. The measurement of the phase shift (Eq. 6), on the other hand, is expected to be insensitive to amplifier gain factors, offset errors and the input power.

IV. Measurement Setup

The silicon chip is glued onto a printed circuit board (PCB) and electrically contacted by wire bonds. This PCB is mounted in the test fixture, with O-rings sealing the gas compartment. The PCB is connected to the MFIA Impedance Analyzer from Zurich Instruments, which also has the full functionality of a lock-in amplifier. This makes it possible to efficiently filter noise and AC voltages of undesired frequencies. The analog voltage output of the MFIA is used to drive the heater voltage with varying frequencies. The response of the thermopiles is evaluated at twice the excitation frequency and applied to the input of the lock-in amplifier. For the measurement, different gases at room temperature are guided into the measuring chamber with mass flow controllers. Before the frequency scan is performed, the chamber is sufficiently flushed with the gas to be analyzed. In this way, we ensure that a complete gas exchange has taken place within the measurement chamber. Afterwards the pressure in the measuring cell is adjusted with a pressure regulator (Fig. 4). For the measurement, the gas supply to the measuring chamber is closed and a frequency scan is performed in the range of 5-200 Hz. Thereby 60 evenly distributed measuring points of the amplitude $U_{Tp,AC}$ and the phase shift Θ of the thermopile signal are recorded on a logarithmic scale. The measurement time for the scan is about 30 seconds.

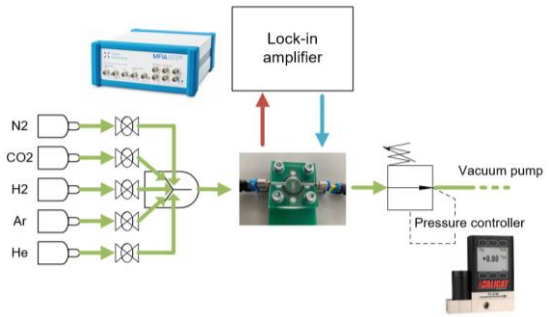

Fig. 4. Schematic overwiew of the meausrement setup: The output voltage is provided by the lock-in amplifier and directly used to excite the heating element. The different gases are provided by MFCs to the measurement chamber. A downstream pressure controller is used to adjust the pressure inside the chamber. The resulting thermopile signal is read out and analyzed by the lock-in amplifier.

V. Experimental Results

In this section, experimental results of different pure gases with dissimilar thermal gas properties are presented. For this purpose, the gases from Table 1 are used, whose thermal conductivity differs from 16.2 to 183.4 mW m^{-1} K^{-1}. At the same time, different volumetric heat capacities are realized by pressure changes, covering a range between 0.42 and 3.11 kJ m^{-3} K^{-1}. With the different thermo-physical gas properties, the performance of the proposed lumped element model can be evaluated over a wide range. We are aware that the gas properties are temperature-dependent [25]. However, we assume that the temperature increase in the chamber is rather small and therefore use for the following analysis gas properties at room temperature for the sake of simplicity. Unless stated otherwise, we always use an excitation voltage with an amplitude of 4 V_{pk}.

A. Thermopile Signals in the Frequency Domain

Figure 5 plots the amplitude of the thermopiles for different gases as a function of frequency. These response curves reveal the characteristic behavior of a low-pass filter. By evaluating such signals, the influence of the gas properties on the thermal equivalent parameters can be studied by a least-square fitting with our lumped model (Eq. 5+6).

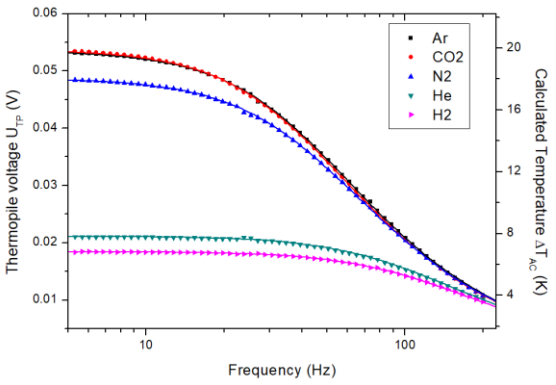

Fig. 5. Single-sided thermopile signal U_{TP} for different gases is showing a low-pass behavior. In order to determine the equivalent parameter, we performed a least square fitting of the thermopile amplitude and assume a Seebeck coefficient of 90 µV/K for Al-polysilicon.

B. Thermal Impedance

Figures 6 and 7 show the lumped parameters, R_{th} and C_{th} as a function of the relevant gas properties. The thermal resistance depends exclusively on the thermal conductivity of the gas. Pressure changes leading to a change in the volumetric heat capacity reveal no change in the fitted thermal resistance. The lower the thermal conductivity of the gas in the measurement chamber, the higher the obtained thermal resistance. In this range the sensor shows the highest sensitivity to changes in thermal conductivity. The correlation between the individual measured values can be fitted with a parallel circuit consisting of two resistors. Here, a gas-dependent thermal resistance with thermal conductivity k (mW m^{-1} K^{-1}) is combined with a gas-independent parasitic thermal resistance (Eq. 7). For the parasitic resistance of our device and layer composition, we calculate a resistance of 4500 K/W using the material parameters from [32]. This value is only 20% larger than the experimentally determined value. The thermal resistance of air $R_{th,air}$, according to our approach,

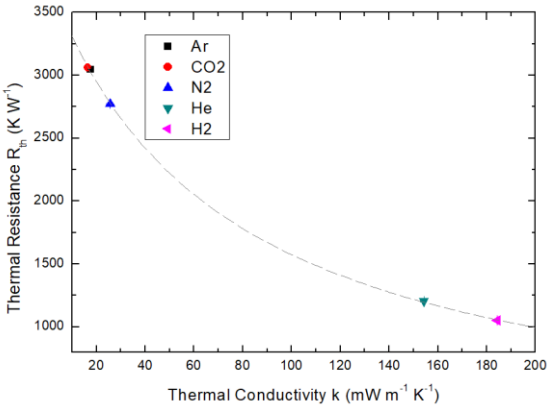

Fig. 6. Thermal resistance R_{th} as a function of the thermal conductivity of the surrounding gas. The influence of the gas thermal conductivity can be modeled with a parallel arrangement of a constant parasitic resistance $R_{th,parasitic}$ and a gas-dependent resistance $R_{th,gas}$ (Eq. 7) resulting in a coefficient of determination of 0.99998.

gives a value of $1.04 \cdot 10^4$ K W^{-1}, which is the same order of magnitude as in [30] indicating that our results may be plausible.

$$R_{th} = R_{th,parasitic} || R_{th,gas}(k) = \left(\frac{1}{3775} + \frac{k}{2.7 \cdot 10^5} \right)^{-1} \qquad (7)$$

Comparing the two thermal resistances and considering an almost static excitation of the heater ($f \rightarrow 0$), it appears that for gases with low thermal conductivity (e.g., Ar, CO_2, N_2) the parasitic heat transport is the dominant mechanism. Consequently, only for gases with a thermal conductivity higher than 72 mW m^{-1} K^{-1} most of the generated heat flows into the gas.

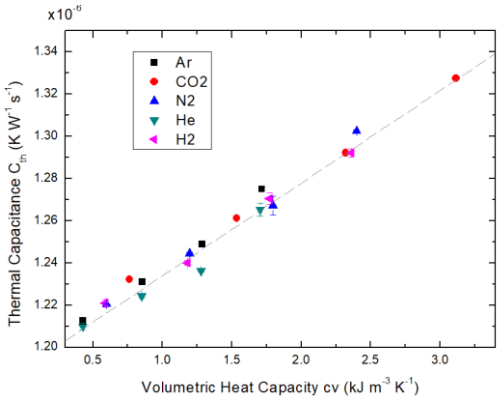

Fig: 7. Thermal capacitance C_{th} as a function of the volumetric heat capacity of the surrounding gas. The influence of the thermal conductivity of the gas on the thermal resistance can be modeled with a parallel connection of a constant parasitic capacity $C_{th,parasitic}$ and a gas-dependent capacity $C_{th,gas}$ (Eq. 8) resulting in a coefficient of determination of 0.98937.

The resulting thermal capacitance of the system, on the other hand, is proportional to the volumetric heat capacity of the gas. Changes in the volumetric heat capacity were realized by pressure changes. A linear dependency of the thermal capacitance with the volumetric heat capacity cv (kJ m^{-3} K^{-1}) of the gas is visible, which can be described by equation 8. At atmospheric pressure conditions, the solid material's heat capacity is clearly dominant. Therefore, for a first estimation of the dynamic behavior of the thermal device, it is legitimate

to neglect the gas influence. This has been done in the past with similar membrane-based sensing structures [17, 30, 33].

$$C_{th} = C_{th,parasitic} + C_{th,gas}(cv) = 1.19 \cdot 10^{-6} + 4.43 \cdot 10^{-8} \cdot cv \quad (8)$$

Nevertheless, we are able to discriminate gases with different volumetric heat capacities. Although gases such as H_2 and N_2 differ significantly in thermal conductivity, the volumetric heat capacity is similar. Ar and CO_2, on the other hand, whose thermal conductivities differ only slightly, can be clearly distinguished by identifying the volumetric heat capacity.

C. Phase Shift

According to equation 6, the product of R_{th} and C_{th} influences the phase shift. Therefore, it is not possible to determine the two thermal equivalent parameters independently. Figure 8 presents the phase shift for various gases with different thermal conductivities evaluated at an excitation frequency of 20 Hz in the pressure range from 500 to 2000 mbar. For comparison, the phase shift (Eq. 6) is plotted with the calculated thermal parameters R_{th} and C_{th} from equations 7 and 8. Here, we do not consider the influence of the heat capacity of the gas and assume that C_{th} is determined only by the parasitic capacitance. In figure 8, the error bar is largest for CO_2 because of its highest volumetric heat capacity. The dependence is also illustrated in figure 9 in which the relative phase change is plotted for gases with relatively similar thermal conductivity as a function of pressure. As expected, Ar shows the smallest change here, since the volumetric heat capacity is the lowest.

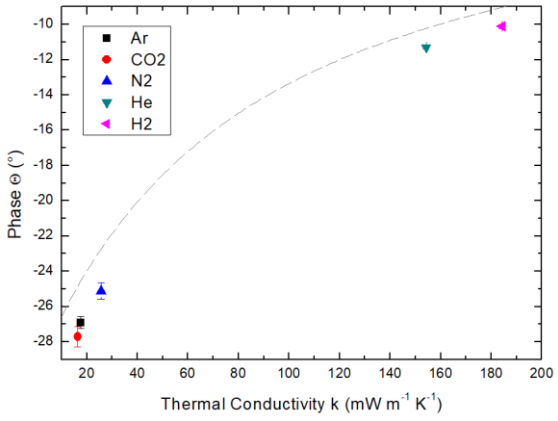

Fig. 8. Phase shift for different gases as a function of thermal conductivity evaluated at an excitation frequency of 20 Hz. For gases with low thermal conductivity and high volumetric heat capacity, larger absolute errors are shown due to the influence of the induced pressure variations.

In general, phase analysis is most suitable for gases that have similar volumetric heat capacities (e.g. Ar and He or N_2 and H_2) and for applications that are subject to only small pressure variations. In cases with large pressure changes, on the other hand, the influence of the volumetric heat capacity on the heat capacity of the sensor system cannot be neglected to accurately distinguish gases based on their thermal conductivity.

D. Signal Sensitivity to Variations in Power Dissipation

Our model (section III) assumes that the phase shift is independent of the applied power, while a measurement of the gas properties based on the amplitude signal requires precise

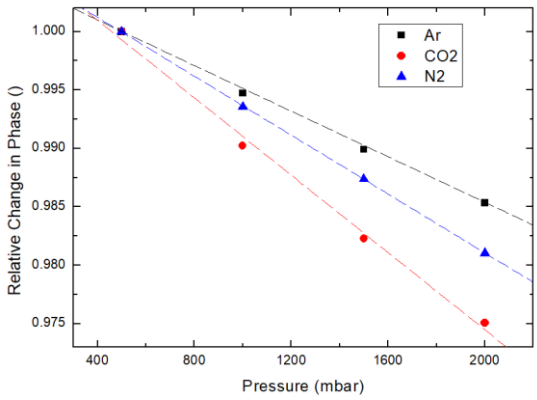

Fig. 9. Relative change in phase as a function of pressure for gases with similar thermal conductivities evaluated at an excitation frequency of 20 Hz. The different sensitivities result from the different volumetric heat capacities of the gases.

knowledge of the dissipated power. Figure 10 displays the relative change in amplitude and phase shift as a function of the excitation voltage. For this purpose, measurements of N_2 at an excitation frequency of 20 Hz are evaluated. By changing the driving voltage within ±7.5 %, the power dissipation changes by ±15 %. The change in amplitude is proportional to the power variation, while the phase signal varies by less than ±0.2 %. These small variations may be caused by the temperature dependence of the thermal conductivity. As a result, the demands on the electronic is reduced when using a phase interpretation, since fluctuations in power dissipation and amplifier gain factors have less influence on the measurement.

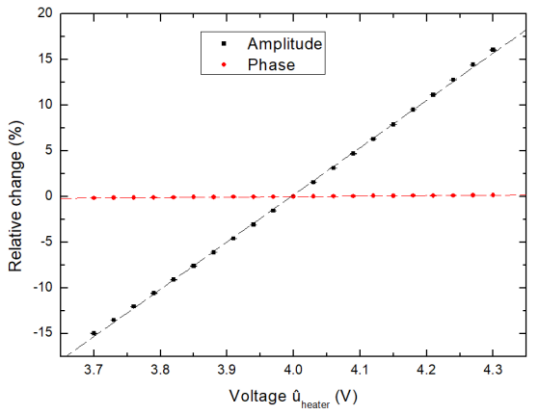

Fig. 10. Relative changes in amplitude and phase of the thermopile signal as a function of varying voltage amplitude for pure N_2 and an excitation frequency of 20 Hz.

VI. Conclusion

This paper has presented a thermal gas sensor that can be employed to simultaneously quantify the thermal conductivity and volumetric heat capacity of pure gases. We have interpreted the gas-dependent temperature response of a heater with a thermal lumped model to estimate these independent thermo-physical gas properties. The applied model for the analysis of the heat loss of a periodically excited heater to the surroundings represented a first order low-pass behavior. An evaluation of the amplitude of the frequency-dependent thermopile signal allowed us to identify the equivalent parameters of our lumped model as a function of the respective gas properties. Here, a high agreement between

the measurement and our predefined lumped model was observed. The approach of fitting the thermopile amplitude and a subsequent interpretation of the frequency-dependent and -independent part is particularly suitable for distinguishing gases with similar thermo-physical properties. For example, CO_2 and Ar could be clearly identified due to their significantly different volumetric heat capacities. In addition to an analysis of the thermopile amplitude, we also examined the respective phase response. Although no individual information about the two thermal gas properties can be obtained, the signal was independent of the applied power. If gases and their mixtures have similar volumetric heat capacities (e.g. H_2 and N_2) and are not exposed to pressure changes in the application, the interpretation of the phase response of the thermopile signal is a promising method to distinguish gases based on their thermal conductivities.

Based on these early results, novel miniaturized thermal sensors with improved performances in sensing individual gas properties will be developed. In this way, we hope to address upcoming applications in the field of hydrogen technologies and smart gas metering with low-cost sensing solutions. Due to the increasing complexities, these applications require the detection of more than one thermo-physical gas property to improve sensitivity, selectivity, and gas specificity.

REFERENCES

[1] M. I. A. Asri, Md. N. Hasan, M. R. A. Fuaad, Y. Md. Yunos, and M. S. M. Ali, "MEMS Gas Sensors: A Review," IEEE Sensors Journal, vol. 21, no. 17, pp. 18381–18397, Sep. 2021.

[2] T. Aldhafeeri, M.-K. Tran, R. Vrolyk, M. Pope, and M. Fowler, "A Review of Methane Gas Detection Sensors: Recent Developments and Future Perspectives," Inventions, vol. 5, no. 3, p. 28, Jul. 2020.

[3] R. Ghosh, J. W. Gardner, and P. K. Guha, "Air Pollution Monitoring Using Near Room Temperature Resistive Gas Sensors: A Review," *IEEE Transactions on Electron Devices*, vol. 66, no. 8, pp. 3254–3264, Aug. 2019.

[4] H. Nazemi, A. Joseph, J. Park, and A. Emadi, "Advanced Micro- and Nano-Gas Sensor Technology: A Review," *Sensors*, vol. 19, no. 6, p. 1285, Mar. 2019.

[5] C. Wang, L. Yin, L. Zhang, D. Xiang, and R. Gao, "Metal Oxide Gas Sensors: Sensitivity and Influencing Factors," Sensors, vol. 10, no. 3, pp. 2088–2106, Mar. 2010.

[6] H. Liu, L. Zhang, K. Li, and O. Tan, "Microhotplates for Metal Oxide Semiconductor Gas Sensor Applications—Towards the CMOS-MEMS Monolithic Approach," Micromachines, vol. 9, no. 11, p. 557, Oct. 2018.

[7] V. Aroutiounian, "Metal oxide hydrogen, oxygen, and carbon monoxide sensors for hydrogen setups and cells," *International Journal of Hydrogen Energy*, vol. 32, no. 9, pp. 1145–1158, Jun. 2007.

[8] Y. Jian *et al.*, "Gas Sensors Based on Chemi-Resistive Hybrid Functional Nanomaterials," *Nano-Micro Letters*, vol. 12, no. 1, Mar. 2020.

[9] P. Srinivasan, M. Ezhilan, A. J. Kulandaisamy, K. J. Babu, and J. B. B. Rayappan, "Room temperature chemiresistive gas sensors: challenges and strategies—a mini review," *Journal of Materials Science: Materials in Electronics*, vol. 30, no. 17, pp. 15825–15847, Aug. 2019.

[10] S. M. Majhi, A. Mirzaei, H. W. Kim, S. S. Kim, and T. W. Kim, "Recent advances in energy-saving chemiresistive gas sensors: A review," *Nano Energy*, vol. 79, p. 105369, Jan. 2021.

[11] T. Hübert, L. Boon-Brett, G. Black, and U. Banach, "Hydrogen sensors – A review," *Sensors and Actuators B: Chemical*, vol. 157, no. 2, pp. 329–352, Oct. 2011.

[12] R. Frodl and T. Tille, "A High-Precision NDIR CO_2 Gas Sensor for Automotive Applications," *IEEE Sensors Journal*, vol. 6, no. 6, pp. 1697–1705, Dec. 2006.

[13] J. Hodgkinson, and R. P. Tatam, "Optical gas sensing: a review," *Measurement Science and Technology*, vol. 24, Nov. 2012.

[14] M. Xu et al., "A design of an ultra-compact infrared gas sensor for respiratory quotient (qCO2) detection," Sensors and Actuators A: Physical, vol. 331, p. 112953, Nov. 2021.

[15] T. A. Vincent and J. W. Gardner, "A low cost MEMS based NDIR system for the monitoring of carbon dioxide in breath analysis at ppm levels," Sensors and Actuators B: Chemical, vol. 236, pp. 954–964, Nov. 2016.

[16] K. Kliche, G. Kattinger, S. Billat, L. Shen, S. Messner, and R. Zengerle, "Sensor for Thermal Gas Analysis Based on Micromachined Silicon-Microwires," *IEEE Sensors Journal*, vol. 13, no. 7, pp. 2626–2635, Jul. 2013.

[17] Z. Cai, R. van Veldhoven, H. Suy, G. de Graaf, K. A. A. Makinwa, and M. A. P. Pertijs, "A Phase-Domain Readout Circuit for a CMOS-Compatible Hot-Wire CO2 Sensor," *IEEE Journal of Solid-State Circuits*, vol. 53, no. 11, pp. 3303–3313, Nov. 2018.

[18] D. Berndt et al., "MEMS-based thermal conductivity sensor for hydrogen gas detection in automotive applications," Sensors and Actuators A: Physical, vol. 305, p. 111670, Apr. 2020.

[19] G. de Graaf and R. F. Wolffenbuttel, "Surface-micromachined thermal conductivity detectors for gas sensing," IEEE Xplore, May 2012.

[20] U. Hammerschmidt, C. Sosna, A. Benkert, A. Meier, and F. Völklein, "A novel single-short-pulse MEMS upstream thermal flow sensor for gases also measuring thermal conductivity and thermal diffusivity," *Sensors and Actuators A: Physical*, vol. 295, pp. 23–30, Aug. 2019.

[21] H. Ernst, A. Jachimowicz, and G. Urban, "Dynamic thermal sensor - principles in MEMS for fluid characterization," *IEEE Sensors Journal*, vol. 1, no. 4, pp. 361–367, Dec. 2001.

[22] J. Kuntner, F. Kohl, and B. Jakoby, "Simultaneous thermal conductivity and diffusivity sensing in liquids using a micromachined device," *Sensors and Actuators A: Physical*, vol. 130–131, pp. 62–67, Aug. 2006.

[23] S. Gauthier, A. Giani, and P. Combette, "Gas thermal conductivity measurement using the three-omega method," Sensors and Actuators A: Physical, vol. 195, pp. 50–55, Jun. 2013.

[24] D. Berndt *et al.*, "A Robust Miniaturized Gas Sensor for H2 and CO2 Detection Based on the 3ω Method," *Sensors*, vol. 22, no. 2, p. 485, Jan. 2022.

[25] E. W. Lemmon, M. L. Huber, and M. O. McLinden, "NIST Standard Reference Database 23: Reference Fluid Thermodynamic and Transport Properties-REFPROP, Version 9.1," NIST, May 2013.

[26] M. März and P. Nance, "Thermal System Modeling Thermal Modeling of Power-electronic Systems." Accessed: Jan. 26, 2023.

[27] O. Behrmann, T. Lisec, and B. Gojdka, "Towards Robust Thermal MEMS: Demonstration of a Novel Approach for Solid Thermal Isolation by Substrate-Level Integrated Porous Microstructures," Micromachines, vol. 13, no. 8, p. 1178, Aug. 2022.

[28] P. G. Szabó and V. Székely, "Characterization and modeling of electro-thermal MEMS structures," Microsystem Technologies, vol. 15, pp. 1293-1301, Apr. 2009.

[29] A. Pike and J. W. Gardner, "Thermal modelling and characterisation of micropower chemoresistive silicon sensors," Sensors and Actuators B: Chemical, vol. 45, no. 1, pp. 19–26, Nov. 1997.

[30] P. G. Szabó and V. Székely, "Investigation of parallel heat flow path in electro-thermal microsystems," Microsystem Technologies, vol. 17, pp. 533-541, Jan. 2011.

[31] F. Hedrich, K. Kliche, M. Storz, S. Billat, M. Ashauer, and R. Zengerle, "Thermal flow sensors for MEMS spirometric devices," Sensors and Actuators A: Physical, vol. 162, no. 2, pp. 373–378, Aug. 2010.

[32] M. von Arx, O. Paul, and H. Baltes, "Process-dependent thin-film thermal conductivities for thermal CMOS MEMS," *Journal of Microelectromechanical Systems*, vol. 9, no. 1, pp. 136–145, Mar. 2000.

[33] G. de Graaf, H.-W. Wu, and R. F. Wolffenbuttel, "A model for static and dynamic thermal analysis of thin film MEMS structures including the thermal conductivity of the surrounding gas," IEEE Xplore, Apr. 2011.